Protein Science (1995), *4*:747–755. Cambridge University Press. Printed in the USA.

Carbohydrate binding sites in a pancreatic α-amylase–substrate complex, derived from X-ray structure analysis at 2.1 Å resolution

MINXIE QIAN, RICHARD HASER, AND FRANÇOISE PAYAN

LCCMB-CNRS, URA 1296 Université Aix-Marseille II, Faculté de Médecine Nord Bd Pierre Dramard, 13916 Marseille Cedex 20, France

(RECEIVED October 26, 1994; ACCEPTED January 17, 1995)

Abstract

The X-ray structure analysis of a crystal of pig pancreatic α-amylase (PPA, EC 3.2.1.1.) that was soaked with the substrate maltopentaose showed electron density corresponding to two independent carbohydrate recognition sites on the surface of the molecule. Both binding sites are distinct from the active site described in detail in our previous high-resolution study of a complex between PPA and a carbohydrate inhibitor (Qian M, Buisson G, Duée E, Haser H, Payan F, 1994, *Biochemistry 33*:6284–6294). One of the binding sites previously identified in a 5-Å-resolution electron density map, lies at a distance of 20 Å from the active site cleft and can accommodate two glucose units. The second affinity site for sugar units is located close to the calcium binding site. The crystal structure of the maltopentaose complex was refined at 2.1 Å resolution, to an *R*-factor of 17.5%, with an RMS deviation in bond distances of 0.007 Å. The model includes all 496 residues of the enzyme, 1 calcium ion, 1 chloride ion, 425 water molecules, and 3 bound sugar rings. The binding sites are characterized and described in detail. The present complex structure provides the evidence of an increased stability of the structure upon interaction with the substrate and allows identification of an N-terminal pyrrolidonecarboxylic acid in PPA.

Keywords: α-amylase; carbohydrates; starch binding; X-ray structure

α-Amylase (α1,4 glucan-4-glucanohydrolase, EC 3.2.1.1) catalyzes the hydrolysis of α-(1,4) glycosidic linkages of starch components and glycogen. In mammals, α-amylase is present in both salivary and pancreatic secretions. Amino acid sequences for mammalian α-amylases show a high degree of homology (Pasero et al., 1986; Qian et al., 1993). Two refined three-dimensional structures obtained at 2.1 Å resolution have been reported for fungal α-amylases: *Aspergillus niger* acid amylase (Brady et al., 1991) and *Aspergillus oryzae* amylase (Swift et al., 1991). Recently a refined three-dimensional structure at 2.8 Å resolution has been reported for a cereal α-amylase, barley malt α-amylase (Kadziola et al., 1994). One three-dimensional structure refined at 2.1 Å resolution has been reported for a mammalian α-amylase from pig pancreas (Qian et al., 1993). The first atomic description of the interaction between a mammalian α-amylase and its inhibitor has been recently reported with the refined structure at 2.2 Å resolution of the PPA/acarbose complex (Qian et al., 1994).

Porcine pancreatic α-amylase is an endo-type amylase. It catalyzes the hydrolysis of α-(1,4) glucosidic bonds in amylose and amylopectin through multiple attack toward the nonreducing end (Robyt & French, 1970b; Prodanov et al., 1984). Two isoenzymes (PPA I and II) are known for pig pancreatic α-amylase (Cozzone et al., 1970). They have the same molecular weight but differ slightly in amino acid composition and isoelectric point (Kluh, 1981; Pasero et al., 1986).

The enzyme requires one essential calcium ion (Vallee et al., 1959; Steer & Levitzki, 1973) for its structural integrity, and it is activated by chloride ions (Levitzki & Steer, 1974); maximal enzymatic activity occurs around pH 7 (Wakim et al., 1969; Ishikawa et al., 1993). Based upon kinetic studies of the action pattern (Robyt & French, 1970a), it is suggested that the active site of PPA contains five subsites for binding of glucose units. The maltopentaose and higher molecular weight maltodextrin molecules are good hydrolytic substrates (Robyt & French, 1970a). The catalytic efficiency (k_{cat}/K_m) increases with chain length from 2 M^{-1} s^{-1} for maltose up to 1.10^7 M^{-1} s^{-1} for 410-residue amylose (Marchis-Mouren & Desseaux, 1989). By kinetic analysis it has been shown that all of the dextrins have more than

Correspondence to: Françoise Payan, LCCMB-CNRS, URA 1296, Faculté de Médecine Nord Bd Pierre Dramard, 13916 Marseille Cedex 20, France; e-mail: payan@lccmb.cnrs-mrs.fr.

Abbreviations: PPA, pig pancreatic α-amylase; TAKA-amylase, *Aspergillus oryzae* α-amylase; G1, G2, G3, etc., glucose, maltose, maltotriose, and higher molecular weight homologues; RMSD, RMS deviation; *R*-factor = $\Sigma \| F_{obs} | - F_{cal} \| / \Sigma | F_{obs} |$.

one bond cleaved, except G5, which undergoes only cleavage at bond 3, producing G2 and G3 molecules. Maltotriose and maltotetraose molecules are considered to be poor substrates that usually undergo the so-called "bireactions" such as condensation during the hydrolysis process (Robyt & French, 1970a).

Low-resolution X-ray studies using PPA isozyme I crystals soaked with methyl and nitrophenyl thiomaltoside revealed two binding sites per molecule for short substrate analogues, the active site was localized, and a second binding site was identified 20 Å away, on the surface of the molecule (Payan et al., 1980).

We have reported in detail the structure of the free enzyme at 2.1 Å resolution (Qian et al., 1993). The crystal structure of the complex between PPA and a carbohydrate inhibitor acarbose was determined at 2.2 Å resolution (Qian et al., 1994). It revealed in detail the arrangement of the protein residues related to the five subsites and it provided the atomic description of the interactions and conformational changes in the enzyme upon inhibitor binding. Many protein/inhibitor hydrogen bond interactions were observed in the complex structure, as was clear hydrophobic stacking of aromatic residues with the inhibitor surface. The chloride activator ion was located in close proximity to the inhibitor. No other carbohydrate unit was found to bind elsewhere on the enzyme molecule.

In the present study, the three-dimensional structure of native PPA soaked with the substrate maltopentaose has been determined to 2.1 Å resolution (Kinemage 1). Our X-ray analysis revealed a well-defined density corresponding to a disaccharide ligand bound at the "second site" and an independent glucopyranose density located on the surface, in close proximity to the calcium ion. The X-ray model clearly presents a subset of residues directly involved in binding the mono- and disaccharide molecules and the important role of the tryptophan residues at the surface of the molecule for sugar-protein docking interactions. The present study also shows that, upon interaction with the substrate, the structure is stabilized and the solvation shield is changed.

Results

Difference electron-density map and quality of the model

As usual, in order to substantiate further discussion, it is important to verify the quality of the structure on which the discussion is to be based.

Initial difference Fourier showed clear density corresponding to a disaccharide maltose ligand in the so-called "second" binding site. No electron density corresponding to a carbohydrate ligand was found in the active site, whereas a monosaccharide unit was clearly identified bound at a site 17 Å from the active-site cleft, in a slight depression on the surface of the molecule, in proximity to the calcium binding site. The density for the three glucopyranose units was well defined, the refinement was done with full occupancy for each of them, corresponding to reasonable individual atomic B values (around 30 Å^2). The final electron density maps for the mono- and disaccharide ligands are shown in Figures 1 and 2, respectively.

The overall conformation of the protein in the present amylase/substrate complex is essentially the same as in the native structure (Qian et al., 1993). In the present structure, none of the structural changes observed in the PPA/acarbose complex crystal (Qian et al., 1994) are detected in the active site and especially the flexible loop between residues 304 and 309 shows the free enzyme conformation. At the 1σ level of the final $(2F_{obs} - F_{calc})\exp(i\alpha_{calc})$ map, all atoms of the model have well-defined density and, moreover, the interaction with the substrate induces stronger electron densities for the residues that showed poor definition in the uncomplexed PPA structure. Especially, all atoms at the N-terminal end are perfectly defined. The quality of the model is demonstrated in Figure 3, showing the observed electron densities for residues 1–4. Our results clearly reveal the nature of the N-terminal residue corresponding to a pyrrolid-2-one-5-carboxylic acid. In the reported amino acid sequence (Kluh, 1981), it is noticed that the N-terminal glutamine was never observed at any stage of the preparation, and they concluded that a cyclization of glutamine to pyrrolidonecarboxylic acid occurred. This feature is clearly observed in the crystal after the enzyme/substrate interaction. Only a few side-chain atoms are not seen in the electron density. Density for Trp 134 does not show CZ2 and CZ3; Lys 142 does not have density beyond CD. Lys 185 has density for the whole side chain, only NZ is not seen; in the same way, the residue Lys 243 does not show density for the atom CE, Asn 363 does not show the ND2 atom, Gln 435, the oxygen atom, and lastly, density for residue Glu 484 does not show the CB–CD bond.

Thermal parameters for the bound sugar ring atoms differ between the two surface binding sites. The mobility of the monosaccharide unit that lies on the surface is significantly higher (mean B value: 37 Å^2) than that of the disaccharide maltose

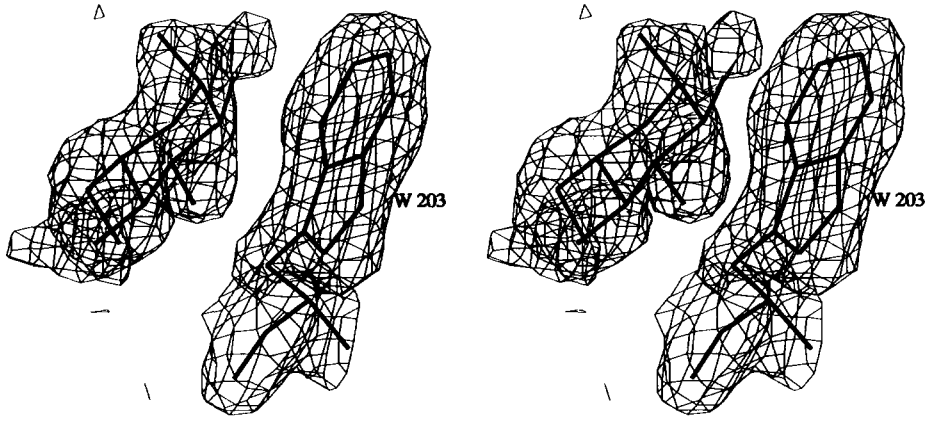

Fig. 1. Stereo view of the final $(2F_{obs} - F_{calc})\exp(i\alpha_{calc})$ electron-density map of the bound monosaccharide at 2.1 Å resolution.

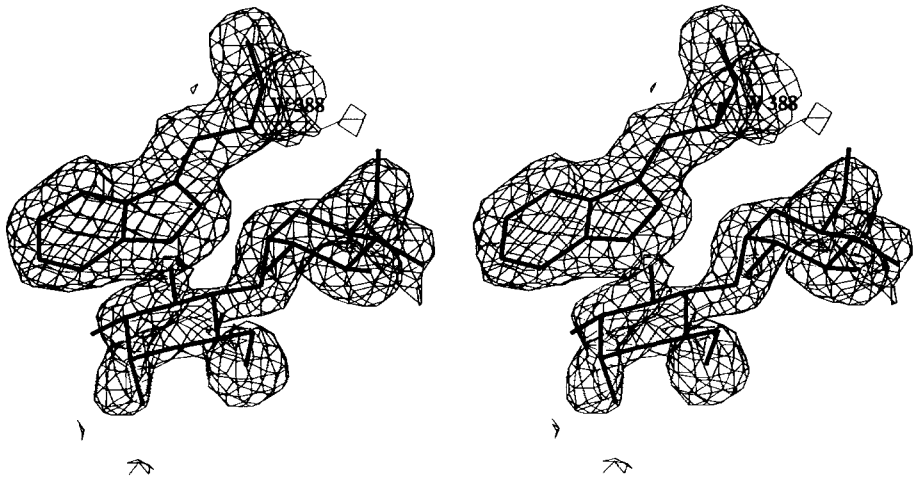

Fig. 2. Stereo view of the final $(2F_{obs} - F_{calc})\exp(i\alpha_{calc})$ electron-density map of the bound disaccharide at 2.1 Å resolution.

(mean B value: 29 Å^2). The mobility of the bound sugar molecules may be correlated with the binding affinity of the sites in which they are located. It is noticeable that the B-factor values observed in this study are markedly higher than those (ranging from 2 to 18 Å^2) exhibited by the atoms of the sugar rings bound at the active site, in the PPA/acarbose interaction (Qian et al., 1994).

The surface binding sites

The current high-resolution study reveals in detail the interactions between the disaccharide and monosaccharide ligands and the mammalian α-amylase. Figures 4 and 7 and Kinemage 1 show the arrangement of amino acid side chains involved in an interaction with the sugar units in each of the binding sites. Table 1 lists major contacts in the protein–carbohydrate interactions.

Arginine, glutamic, and aspartic polar–planar side chains, main-chain polar groups, and the ammonium side chain of two lysine residues form the first shell of the network of hydrogen bonds around the bound sugar units. As usually observed in protein–carbohydrate interactions (Vyas, 1991), the hydrogen bonded network is completed by water molecules mediating indirect contacts between carbohydrate and protein. Another major feature of the protein–sugar interactions (Quiocho, 1989) also observed in the active site of PPA (Qian et al., 1994) is found in both of the surface binding sites of the G5 complex. Indeed, clear hydrophobic stacking of the aromatic residues occurs, involving the indole ring of Trp residues (Trp 203 and Trp 388) abutting one glucose ring of the oligosaccharide ligand (Kinemage 1). It should be noted that stacking interactions between sugar and aromatic residues occur in all known surface binding sites of α-amylases (present study; M. Qian & F. Payan,

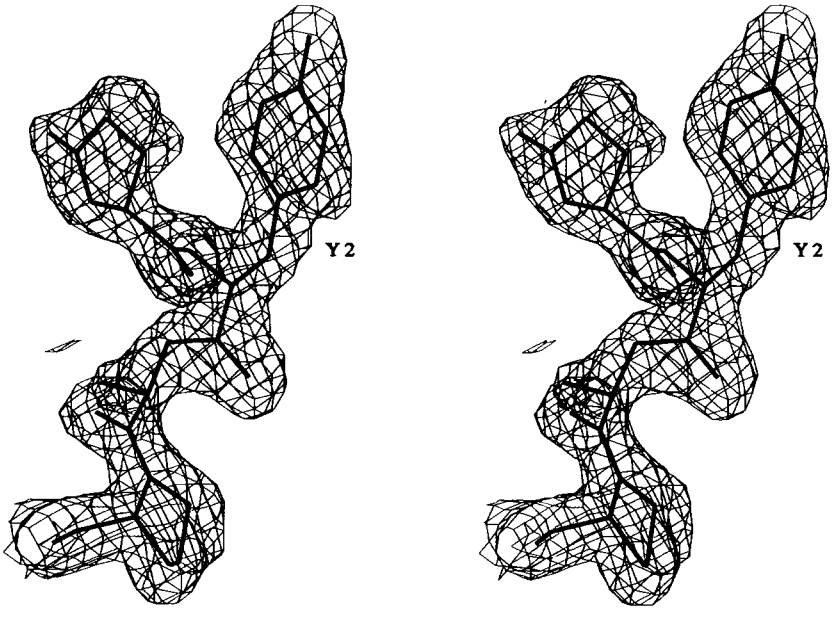

Fig. 3. Quality of the final $(2F_{obs} - F_{calc}) \times \exp(i\alpha_{calc})$ electron-density map at 2.1 Å resolution as exemplified at residues 1–4. Density for the N-terminal pyrrolidonecarboxylic acid is also shown.

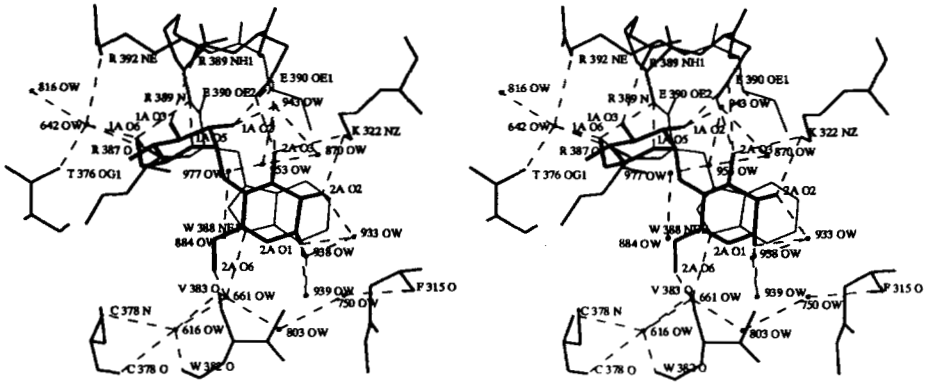

Fig. 4. Detailed stereo view of arrangement of protein side chains involved in interaction with the disaccharide maltose.

unpubl. results) and other amylolytic enzymes such as CGTase from *Bacillus circulans* Strain 251 (Lawson et al., 1994).

Interactions in the maltose binding site

The site henceforth referred to as the "second site" is located at the interface between the so-called domains A and C of our free enzyme structure (Qian et al., 1993).

The torsion angles at the α-(1,4)-*O*-glycosidic bonds connecting sugar residues 1A and 2A (Fig. 4) are close to the minimum energy values allowing formation of O2–O3′ hydrogen bonds between adjacent sugar residues, which is characteristic of maltose and amylose crystals (Johnson et al., 1988). The disaccharide in approximate helical conformation curls toward the protein, abutting against the aromatic side chain of the residue Trp 388, and then away. The nonpolar cluster, C2-H, C4-H (residue 2A),

Table 1. *Protein–oligosaccharide interactions in the PPA/maltopentaose complex*[a]

Sugar Site	Polar contacts with protein			Water-mediated polar contacts with protein			
	Sugar atom	Protein atom	Distance (Å)	Water	Protein	Distance (Å)	Geometry of the glycosidic linkage
1A	O2	Glu 390 OE1	2.9	(Ow 642)	Ow 816	2.8	1A to 2A: $\Phi = 101.8$; $\Psi = -157.8°$
	O2	Ow 943*	3.2	(Ow 642)	Arg 387 O	2.7	
	O3	Arg 389 NH1	2.6	(Ow 642)	Arg 392 NE	3.1	O2(1A)–O3(2A) = 2.94 Å
	O5	Arg 389 N	2.9	(Ow 642)	Thr 376 OG1	2.7	
	O6	Arg 389 N	2.8	(Ow 943*)	Ow 953*	2.7	
	O6	Arg 387 O	2.7	(Ow 953*)	Ow 977*	2.9	
	O6	Ow 642	3.1	(Ow 977*)	Ow 884*	2.6	
2A	O1	Ow 939*	2.6	(Ow 943*)	Ow 870*	2.9	
	O1	Ow 933*	2.7	(Ow 953*)	Ow 870*	2.8	
	O1	Ow 938	2.8	(Ow 661)	Trp 388 Ne	3.0	
	O2	Lys 322 NZ	2.8	(Ow 661)	Val 383 O	2.8	
	O2	Ow 933*	3.1	(Ow 661)	Ow 803	3.0	
				(Ow 803)	Ow 750	2.6	
	O3	Lys 322 NZ	2.9	(Ow 750)	Phe 315 O	3.0	
	O3	Glu 390 OE1	3.2	(Ow 661)	Ow 616	2.9	
	O3	Glu 390 OE2	3.1	(Ow 616)	Cys 378 O	3.0	
	O6	Ow 661	2.6	(Ow 616)	Cys 378 N	3.0	
				(Ow 616)	Val 383 O	3.1	
				(Ow 616)	Trp 382 O	2.9	
3A	O1	Ow 896*	2.8	(Ow 577)	Ow 556	2.7	Monosaccharide
	O2	Lys 140 NZ	3.1	(Ow 556)	Asn 137 ND2	2.9	
	O3	Lys 140 NZ	3.1	(Ow 556)	Asp 159 OD2	2.8	
	O3	Ow 577	2.6	(Ow 556)	Ow 539	3.0	
	O4	Asp 206 OD2	2.7	(Ow 539)	Ca^{2+}	2.4	
	O4	Ow 910*	3.0				
	O6	Asp 206 OD2	3.3				
	O6	Asp 206 N	3.2				
	O6	Ow 619	2.9	(Ow 619)	Gly 205 N	2.8	

[a] Φ is the torsion angle about C1(1A)–O4(2A), defined by O5(1A)–C1(1A)–O4(2A)–C4(2A); Ψ is the torsion angle about O4(2A)–C4(2A), defined by C1(1A)–O4(2A)–C4(2A)–C5(2A); *, only present in the complexed state.

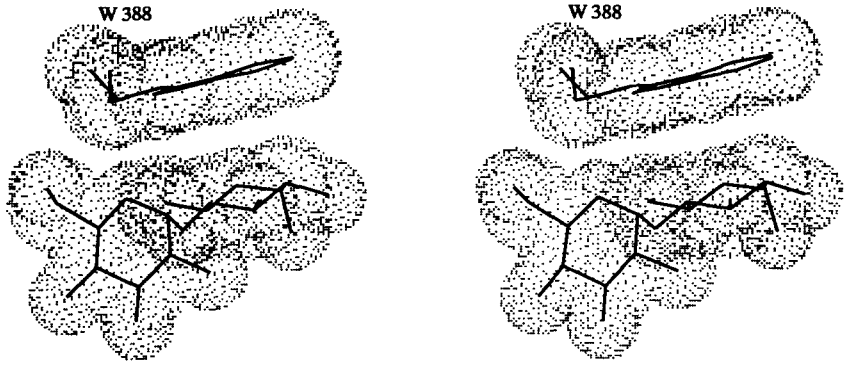

Fig. 5. Stacking feature between the plane of the tryptophan ring of residue 388 and the hydrophobic region of the maltose unit bound at the "second site" of the enzyme molecule. Dotted surface represents the van der Waals radii of the atoms.

and C1′-H (residue 1A), stacks directly below the plane of the indole ring of Trp 388, making a clear hydrophobic interaction (Figs. 4, 5). The indole ring of the tryptophan is nearly parallel to the 2A-sugar's surface. The binding site architecture is completed by a triad of residues Glu 390, Arg 389, and Lys 322, which acts like pincers to dock the disaccharide maltose (Fig. 4; Table 1).

The binding interactions are formed by residues from the N-terminus helical segments of the Aα7 and Aα8 helices of the domain A $(\beta/\alpha)_8$ barrel (notation according to Qian et al., 1993). However, as shown on Figure 6 and Kinemage 1, the binding site is located in a surface area of domain A, facing the loop segment between strands Cβ9 and Cβ10 of the domain C, in the immediate neighborhood of the interface region between the domains A and C. This interface is formed by juxtaposition of one sheet of the domain C, including the strands Cβ1, Cβ2, Cβ3, and Cβ10, facing the α-helices Aα7 and Aα8. In the crystal lattice, the bound disaccharide appears further stabilized by van der Waals interaction with the residue Trp 134 (domain B) of a contiguous symmetric enzyme molecule. The binding region of the reference molecule is contiguous to the B domain of a symmetry-related molecule and consequently not far from its active-site cleft. In the disaccharide binding region, the protein residues make no movement and appear to be in the right orientation to accept the disaccharide; however, a slight structural rearrangement is observed in a nearby cluster of residues, namely, Glu 484 (from the loop between the strands Cβ9 and Cβ10 of the reference molecule) and Trp 134 from the domain B of a symmetry-equivalent molecule. The side chain of residue Trp 134, protruding in the solvent (Fig. 6), moves, coming within van der Waals distance of the bound sugar 2A of the disaccharide ligand, whereas the whole residue Glu 484 shows a small movement away from the binding region; the mobility of these two residues can be related to the disordered side chains we observed in the electron density and their high *B*-factor values in the free and complexed PPA structures.

The glucopyranose binding site

The current study clearly reveals in detail the interactions between the mammalian α-amylase and a glucose ring lying almost on the surface, anchored at the entrance of an open depression at the bottom of which the calcium ion (Qian et al., 1993) is enmeshed. Figure 7 and Kinemage 1 show the arrangement of protein side chains and calcium ion involved in interaction with the glucopyranose unit. This bound saccharide ring has the common $^4C_1$ full chair conformation. It forms interactions (Table 1) with the loop segment 138–145 of the domain B and the initial amino-terminal turn of α-helix 4 of the domain A $(\beta/\alpha)_8$ barrel. It lies directly above the plane of the indole ring of residue Trp 203 (Figs. 1, 7), its A face with a hydrophobic patch composed of C2 and C4 is directed toward the aromatic ring. This packing configuration is similar to that observed for the glucose

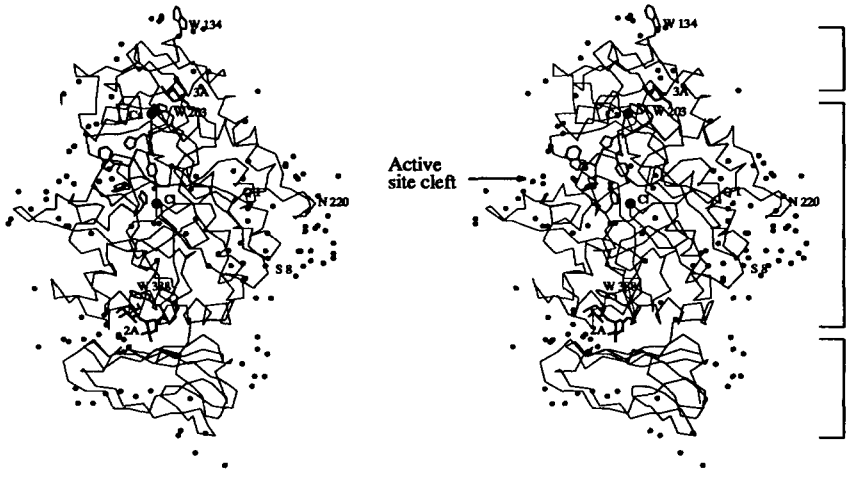

Fig. 6. Stereo diagram of the α-carbon tracing of the G5/PPA complex molecule showing the distribution of the bound water molecules only present in the complexed state. Chloride and calcium ions are shown in close proximity to the active-site cleft. Monosaccharide and disaccharide ligands, 3A and 2A respectively, are shown. Hydrophobic residues identified in the surface binding sites (present study) and those previously identified (Qian et al., 1994) in the active-site interactions are shown. Residue Trp 134 is seen protruding in the solvent at the top edge of the molecule. The N-terminal segment and Asn 220 residues are pointed out.

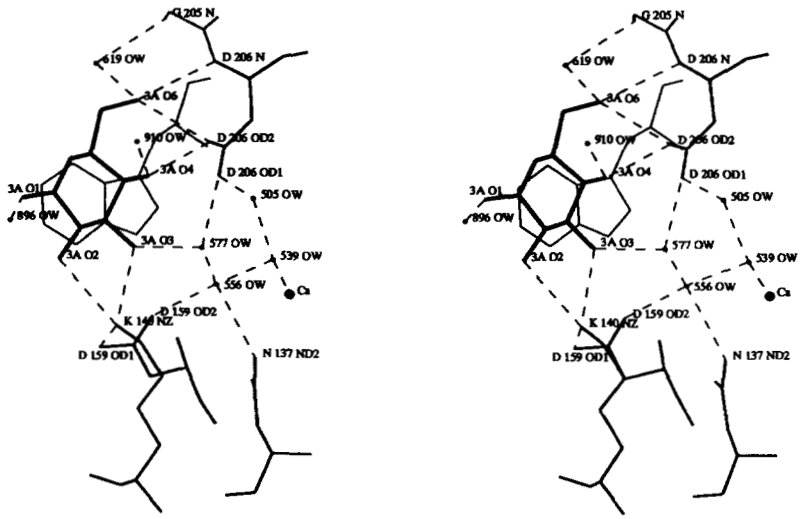

Fig. 7. Detailed stereo view of the arrangement of protein side chains involved in interaction with the monosaccharide. Calcium ion is shown in interaction with the sugar unit through its water molecule ligand.

residue 2A in the "second" site. The glucose residue participates in direct and water-mediated hydrogen bonds with the protein (Table 1). The calcium ion lies at a distance of 9.1 Å from the O3 hydroxyl of sugar ring 3A. As shown on Figure 7, the calcium ligand, 539OW, is hydrogen bonded to O3 through water molecules 556 and 577 already present in the free enzyme structure and which constitute a channel of hydrogen bonded solvent molecules between the calcium ion and the exterior of the enzyme molecule. Thus, in addition to being located 12.4 Å away from the point of the catalytic attack, and involved in a network of interactions with the chloride ion and the catalytic residues (Qian et al., 1994), the calcium ion is in contact, on the opposite side toward the exterior of the enzyme, with a sugar affinity binding site (Fig. 6).

Solvent structure

The final G5 complex model contains 425 ordered water molecules, instead of 353 in the free enzyme molecular model. Inspection of the solvent molecules observed in the free and complexed states indicates that 134 of them are new molecules accompanying the saccharide ligand. They belong to the bulk water and, as shown in Figure 6, they form noticeable clouds in some parts of the molecule. Namely, they are found at the entrance of the active-site cleft in proximity to the flexible loop (304–309) and on the opposite side of the molecule, related to the domain A β-barrel, forming hydrogen bonds with residues from the N-terminal segment. The dense solvation shield observed in the complex structure may be related to the observed increased order for several residues.

Two further areas crowded with new ordered water molecules are observed on the Figure 6—in the "second site" binding region and near the long loop 212–229. In the crystal lattice, these areas are together situated in a pocket between symmetry-equivalent molecules and they create a water molecule network bridging the pocket from hydroxyl oxygens of the disaccharide maltose (1A-O2, 2A-O1) of the reference molecule to the side-chain (OD1 and ND2) and carbonyl oxygen atoms of the residue Asn 220 (see Fig. 6) of the contiguous molecule. This loop follows after the helix Aα4 (residues 203–212) at the N-terminal of which is bound the monosaccharide ring A3 (Fig. 6; Table 1).

It is also noteworthy that the water molecule network that occupies the active-site cleft in the free enzyme structure is disrupted, several of the ordered solvent molecules have disappeared and may be released to the bulk solvent.

As usually observed in protein–carbohydrate interactions (Vyas, 1991), a substantial part of the hydrogen bonding potential of sugar residues is engaged in interactions with water molecules (Table 1). As observed in our previous study of the PPA/inhibitor complex (Qian et al., 1994), several ordered water molecules mediating hydrogen bonds between carbohydrate and protein are new molecules accompanying the sugar residues (Table 1).

Discussion

Disaccharide specificity

Our results show that in the "second" binding site, the ligand residues do not move and appear to be in the right position to accept a maltose molecule in the preferred helical configuration. Maltose binds in the recognition site, making strong interactions through hydroxyl groups from the two glucose units to ionizable residues on the protein. Regardless of which oligosaccharides are used in the binding study (Payan et al., 1980; M. Qian & F. Payan, unpubl. results), only two glucose units are bound. This surface binding site seems designed specifically to bind a disaccharide maltose by demanding contacts to O2 and O3′ hydroxyls of adjacent sugars and the features of the recognition site involve favorable contacts made by bridging the span of a disaccharide. α-Amylase likely exhibits disaccharide specificity, as observed for other enzymes such as phosphorylase at the storage site (Johnson et al., 1988). In CGTase from *Bacillus circulans* Strain 251, a maltose binding site located in domain C has been observed to show similarities with the present binding site of PPA (Lawson et al., 1994). As we proposed earlier (Buisson et al., 1987), this "second" binding site in α-amylases may be an anchorage region for the natural substrates of the enzyme on

their way to the active site. This disaccharide binding probably has to be included in the mechanism of mammalian α-amylases involving a multiple attack.

As already mentioned, G5 is a good hydrolytic substrate, rapidly hydrolyzed by PPA. By kinetic analysis it has been shown that all of the maltodextrins have more than one bond cleaved, except G5, which undergoes only cleavage at bond 3, producing G2 and G3 molecules (Robyt & French, 1970a). The results reported here suggest that, as expected, PPA in the crystal is able to cleave a maltose unit from the reducing end of the initial maltopentaose molecule. The rapid dissociation of the complex concomitant with breakdown of the substrate would account for the lack of density in the active site after the 12 h of the experiment. The released G2 compounds would recognize the disaccharide binding site, giving rise to stable complexes. In the maltose binding region, we observe a conformational flexibility of the residue Trp 134 side chain belonging to the contiguous equivalent molecule in the symmetry operation $(-X, Y-1/2, -Z+1/2)$, a feature indicative of plausible interactions between the protein molecules. In this regard, situation of the residue Trp 134 protruding in the solvent channel, which links the second binding site of a molecule to domain B and to the active site of the neighboring molecule, is of interest. It supports a contribution of this residue in the enzyme/starch interaction. A noticeable ligand-induced conformational change is also observed concerning the loop segment around residue 484, from domain C. Moreover, we have evidence from the G5 complex crystal structure of the existence of a glucopyranose site on the surface of the enzyme molecule located close to the calcium binding site. Although we find only one glucose bound at this recognition site with a docking configuration in fact similar to that observed for the glucose residue 2A in the "second" site, we cannot exclude that a longer oligosaccharide molecule may be present and disordered in the solvent. The existence of this "affinity" site contributes to support the multivalency of α-amylase binding to long amylose chains. All of the above observations converge to promote extensive interactions between the enzyme molecules with the cooperative contribution of multiple binding sites in each of them. That would agree with the deductions from equilibrium dialysis and electron microscopy studies (Loyter & Shramm, 1966), which indicate the existence on the enzyme of at least two apparently independent binding sites for maltotriose molecules (consistent with subsequent crystallographic results; Payan et al., 1980); and the formation of multimolecular complexes when PPA interacts with dextrins.

Possible role of domain C

In the crystal lattice, the β-strands of the Greek key composing the geometry of the domain lie between the "second" site of one molecule and the active site of the contiguous molecule along the a cell parameter direction throughout the crystal. This arrangement might be indicative of some potential role for this β-stranded domain in mediating the attachment of the polysaccharide chains on the molecules. We are not aware of any result in the literature that clearly contributes to the understanding of the role of this C domain lobe. It is worth mentioning that its location in the lattice relative to the active and other sugar binding sites and also its topology, reminiscent of a lectin fold, are features that seem to support a possible mediating role of this domain.

The present study of a PPA/maltopentaose complex provides the evidence of increased stability of the structure upon interaction with the substrate. The solvation shield in the complexed structure is modified compared to that observed at the same resolution for the free enzyme and possibly contributes to the increased stability of the structure. Experiments of limited proteolysis on porcine pancreatic amylase (Desseaux et al., 1991) showed that the short hinge of residues (403–407) joining the domain C to the major α/β domain was not susceptible to a proteolytic attack by subtilisin and other tested proteinases. The free PPA molecule was hydrolyzed by subtilisin specifically at peptide bond 369–370 from a long loop connecting Aβ8 and Aα8, protruding from the barrel and particularly exposed to the solvent. The presence of a ligand bound at the surface site in the vicinity of this region may also provide increased resistance to proteolytic attack; it is noteworthy that the side chain of residue Glu 369, disordered in the free protein structure, protrudes with a well-defined electron density into the solvent.

This thorough analysis of the complexed state of PPA after interaction with its substrate shows the ability of the enzyme molecule to offer multiple carbohydrate binding sites. Nonpolar interactions appear to be an important feature for each of these sites. The enzyme exhibits disaccharide specificity at the "second site."

Materials and methods

Crystals of native PPA used in this study were identical to those previously used for the free enzyme structure determination (Qian et al., 1993) and for the acarbose/enzyme complex structure (Qian et al 1994). Crystal packing (Payan et al., 1980) allows the study of substrate interactions with the enzyme by soaking native crystals in buffered crystal-stabilizing solutions of the compound of interest. Maltopentaose (G5) was purchased from Boehringer Mannheim. In the present study, complexes were formed by soaking crystals for 12 h at 20 °C in a solution containing 10 mM G5 in Tris buffer 0.01 M, 1 mM $CaCl_2$, 2 M NaCl, at pH 8. X-ray diffraction data for the G5 complex crystals were collected using a Mar-Research imaging plate scanner developed by Hendrix and Lentfer (Hamburg). Data were processed and scaled using the XDS program (Kabsch, 1988). The data set for the G5 complex was 94.5% complete up to 2.1 Å resolution, it was 85.5% complete in the final shell with I/σ above 3.0.

The $(F_{obs,complex} - F_{obs,native})\exp(i\alpha_{calc,native})$ maps calculated between 25 and 2.1 Å showed a disaccharide density in the "second" binding site previously identified but not described in our low-resolution studies of PPA with maltotriose analogs (Payan et al., 1980). Initial difference Fourier maps also showed density corresponding to a monosaccharide ring located on the surface, close to the calcium binding site. Initial phases for the complex ($\alpha_{calc,native}$) were calculated from the completely refined model of the native enzyme (Qian et al., 1993).

We used the simulated annealing program XPLOR (Brünger et al., 1987) and followed a protocol similar to the one for the acarbose complex (Qian et al., 1994). The procedure started with the refined structure of uncomplexed PPA after deletion of water molecules located on the surface in the expected second binding site region. The template of a glucose residue for refinement of the ligand structure was taken from crystallographic data for

Table 2. *Statistics of data collection and refinement*

	Native	Complex
Cell parameters ($P2_12_12_1$)		
a (Å)	56.3	56.3
b (Å)	87.8	87.8
c (Å)	103.4	103.4
Resolution limit (Å)	2.06	2.00
No. of measurements	111,419	168,572
Unique reflections	30,390	31,387
Completeness of data set (%)	99	88.7
R_{sym}[a]	4.07	5.3
Refinement range (Å)	8-2.1	8-2.1
No. of reflections in refinement	29,838	27,558
R-factor (%)[b]	15.6	17.5
R_{free}[c]	–	23.3
No. of protein atoms	3,910	3,910
No. of ligand atoms	–	35
No. of water molecules	353	425

	Native	Complex	Di- and monosaccharide
RMSD			
Bond lengths (Å)	0.014	0.007	0.009 and 0.007
Angles (°)			
Temperature factors, $\langle B \rangle$ (Å^2)	2.8	1.4	1.6 and 1.3
Main-chain atoms	12.5	12.7	–
Side-chain atoms	15.8	17.3	29.7 and 37.8
Water molecules	30.5	31.9	–

[a] R_{sym} is defined as $\sum_{i,hkl} |I(i,hkl) - \langle I(hkl)\rangle| / \sum_{i,hkl} I(i,hkl)$, where i runs through the symmetry-related reflections.

[b] Crystallographic R is defined as $\sum |F_o - F_c| / \sum |F_o|$.

[c] $$R_{free} = \frac{\sum_{(h,k,l)\in T} \| F_{obs}(h,k,l)| - k|F_{calc}(h,k,l)\|}{\sum_{(h,k,l)\in T} |F_{obs}(h,k,l)}.$$

individual monosugars. All model construction and structure comparison work used the program TURBO implemented on a Silicon graphics 4D/380 computer (Roussel & Cambillau, 1989).

All solvent molecules with densities below 1σ in the $(2F_{obs} - F_{calc})\exp(i\alpha_{calc})$ map and temperature factors above 70 Å^2 were removed after the first iteration of refinement. The difference electron density map also revealed additional water molecules, though some of the ordered molecules already present in the free enzyme structure disappeared; sites were added to the model provided that the electron density was present at a level of at least 3.5σ in the $(F_{obs} - F_{calc})\exp(i\alpha_{calc})$ maps. The molecules introduced were inspected visually for correct geometry of hydrogen bonding and were given an initial B-factor of 20 Å^2. When the R-factor reached 17.5% in the range 8.0–2.1 Å for 27,558 reflections, with a model obeying standard geometry within 0.007 Å in bond lengths and 1.4° in bond angles, and the $(F_{obs} - F_{calc})\exp(i\alpha_{calc})$ map showed no more interpretable features, refinement was halted, yielding a model consisting of 3,910 protein atoms (i.e., all non-hydrogen atoms), 1 Ca ion , 1 Cl ion, 35 oligosaccharide atoms, and 425 water molecules (Table 2).

Crystallographic coordinates for the PPA structure have been deposited with the Brookhaven Protein Data Bank.

Acknowledgments

This work has been supported by the CNRS-IMABIO program, the ANVAR organism, and by the PACA region.

References

Brady RL, Brzozowski AM, Derewenda ZS, Dodson EJ, Dodson GG. 1991. Solution of the structure of *Aspergillus niger* acid α-amylase by combined molecular replacement and multiple isomorphous replacement methods. *Acta Crystallogr B 47*:527–535.

Brünger AT, Kuriyan J, Karplus M. 1987. Crystallographic *R* factor refinement by molecular dynamics. *Science 35*:458–460.

Buisson G, Duée E, Haser R, Payan F. 1987. The three-dimensional structure of porcine pancreatic α-amylase at 2.9 Å resolution. Role of calcium in structure activity. *EMBO J 6*:3909–3916.

Cozzone P, Pasero L, Marchis-Mouren G. 1970. Characterization of porcine pancreatic isoamylases: separation and amino acid composition. *Biochim Biophys Acta 200*:590–593.

Desseaux V, Payan F, Ajandouz El H, Svensson B, Haser R, Marchis-Mouren G. 1991. Effect of limited proteolysis in the 8th loop of the barrel and of antibodies on porcine pancreas amylase activity. *Biochim Biophys Acta 1080*:237–244.

Ishikawa K, Matsui I, Kobayashi S, Nakatani H, Honda K. 1993. Substrate recognition at the binding site in mammalian pancreatic α-amylases. *Biochemistry 32*:6259–6265.

Johnson LN, Cheetham J, McLaughlin JP, Acharya KR, Barford D, Phillips DC. 1988. Protein-oligosaccharides interactions: Lysozyme, phosphorylase, amylases. *Curr Top Microbiol Immunol 139*:82–134.

Kabsch W. 1988. Automatic indexing of rotation diffraction patterns. *J Appl Crystallagr 21*:67–71.

Kadziola A, Abe J, Svensson B, Haser R. 1994. Crystal and molecular structure of barley α-amylase. *J Mol Biol 239*:104–121.

Kluh I. 1981. Amino acid sequence of hog pancreatic α-amylase isoenzyme I. *FEBS Lett 136*:231–234.

Lawson CL, van Montfort R, Strokopytov B, Rozeboom HJ, Kalk H, de Vries GE, Penninga D, Dijkhuizen L, Dijkstra BW. 1994. Nucleotide sequence and X-ray structure of cyclodextrin glycosyltransferase from *Bacillus circulans* Strain 251 in a maltose-dependent crystal form. *J Mol Biol 236*:590–600.

Levitzki A, Steer ML. 1974. The allosteric activation of mammalian α-amylase by chloride. *Eur J Biochem 41*:171–180.

Loyter A, Schramm M. 1966. Multimolecular complexes of α-amylase with glycogen limit dextrin. *J Biol Chem 241*:2611–2617.

Marchis-Mouren G, Desseaux V. 1989. Structure and function of α-amylases. *Biochem Life Sci Adv 8*:91–96.

Pasero L, Mazzei-Pierron Y, Abadie B, Chicheportiche Y, Marchis-Mouren G. 1986. Complete amino acid sequence and location of the five disulfide bridges in protein pancreatic α-amylase. *Biochim Biophys Acta 869*:147–157.

Payan F, Haser R, Pierrot M, Frey M, Astier JP, Abadie B, Duée E, Buisson G. 1980. The three-dimensional structure of α-amylase from porcine pancreas at 5 Å resolution. The active site location. *Acta Crystallogr B 36*:416–421.

Prodanov E, Seigner C, Marchis-Mouren G. 1984. Subsite profile of the active center of porcine pancreatic α-amylase. Kinetic studies using maltooligosaccharides as substrates. *Biochem Biophys Res Commun 122*: 75–81.

Qian M, Buisson G, Duée E, Haser H, Payan F. 1994. The active center of a mammalian α-amylase. Structure of the complex of a pancreatic α-amylase with a carbohydrate inhibitor refined to 2.2 Å resolution. *Biochemistry 33*:6284–6294.

Qian M, Haser H, Payan F. 1993. Structure and molecular model refinement of pig pancreatic α-amylase at 2.1 Å resolution. *J Mol Biol 231*:785–799.

Quiocho FA. 1989. Protein-carbohydrate interactions: Basic molecular features. *Pure Appl Chem 61*:1293–1306.

Robyt JF, French D. 1970a. The action pattern of porcine pancreatic α-amylase in relationship to the substrate binding site of the enzyme. *J Biol Chem 245*:3917–3927.

Robyt JF, French D. 1970b. Multiple attack and polarity of action of porcine pancreatic α-amylase. *Arch Biochem Biophys 138*:622–670.

Roussel A, Cambillau C. 1989. *Silicon Graphics geometry partner directory (fall 1989)*. Mountain View, California: Silicon Graphics. pp 77–78.

Steer M, Levitzki A. 1973. The metal specificity of mammalian α amylases as revealed by enzyme activity and structural probes. *FEBS Lett 31*:89–92.

Swift HJ, Brady L, Derewenda ZS, Dodson EJ, Dodson GG, Turkenburg JP, Wilkinson AJ. 1991. Structure and molecular model refinement of *Aspergillus oryzae* (TAKA) α-amylase: An application of the simulated-annealing method. *Acta Crystallogr B 47*:535–544.

Vallee BL, Stein EA, Summerwell WN, Fisher EH. 1959. Metal content of α-amylases of various origins. *J Biol Chem 234*:2901–2929.

Vyas NK. 1991. Atomic features of protein–carbohydrate interactions. *Curr Opin Struct Biol 1*:732–740.

Wakim J, Robinson M, Thoma JA. 1969. The active site of porcine pancreatic α-amylase: Factor contributing to catalysis. *Carbohydr Res 10*: 487–503.